ONR Final Technical Report

The Properties of Thermally Passivated $Si_{1-x}Ge_x$ Produced Using High Pressure Techniques

Contract Number: N00014-91-J-1837
R&T Numbers: 4145308---01,02,03

1.0 Project Summary

The focus of this work was the development of high pressure techniques for the electronic and chemical passivation of group IV alloy and compound semiconductor surfaces. The project goals were initially focussed on the use of ultra high pressure oxidation to produce high quality $Si_{1-x}Ge_x$ MOS oxides and were expanded, via an ASSERT award, to include a study of the application of this technique to the oxidation of SiC. High pressure oxidation of $Si_{1-x}Ge_x$ was explored using both high pressure wet (hydrothermal) and dry pure oxygen conditions. A process window was established where the compositionally congruent incorporation of Ge into the oxide was achieved and the kinetics of both wet and dry processes were established within this process window. The physical, chemical, and electrical properties of the resultant oxides were studied using a wide range of analytical techniques. The performance of the high pressure oxides were optimized using a nitride capping layer to reduce current leakage through the oxide. During the course of this research on the formation of high pressure $Si_{1-x}Ge_xO_2$ we developed a new method for the synthesis of nanocrystalline Ge embedded in an SiO_2 matrix. This process was used to fabricate structures that exhibit visible PL. Single crystal films of n-type 3C-SiC were also hydrothermally processed at pressures ranging from 10 to 70 MPa at 550°C and the effects of initial thin film microstructure on final oxide structure was explored. This study revealed that low temperature (T=550°C) oxidation of single crystal epitaxial SiC is possible but that the resulting oxide film microstructure is strongly dependent on the initial film microstructure and oxidation is greatly enhanced along low angle grain boundaries and on planar defects. This contract supported, in part, one PhD candidate, one MSc. candidate, numerous undergraduate research assistants, and at least 8 papers were published in refereed Journals and Proceedings.

2.0 Significant Results

2.1 High Pressure Technique Development

The principal advantage offered by HPO is that the rate of oxidation can be controlled (over a limited temperature range) independent of the reaction temperature by adjusting the oxidant pressure. The importance of this is that in an oxidizing environment under conditions near thermodynamic equilibrium, Si will be selectively removed from

the alloy thus leaving behind a Ge enriched layer at the oxide/alloy interface. If, however, reasonable oxidation rates can be achieved at temperatures that are low enough to kinetically freeze the interdiffusion of Si and Ge, then the oxidation interface (i.e. at the oxide/alloy interface), will no longer be in chemical equilibrium with respect to the Si in the alloy and the oxidation potential can locally increase enough to enable the oxidation of Ge and its incorporation into the growing oxide. Application of higher oxidation pressures at a particular temperature affects the rate of oxidation but not the rate at which the components in the alloy can redistribute and hence it is possible to find conditions where a compositionally congruent oxide is formed from the underlying alloy by simply compensating for a decrease in temperature with an increase in pressure.

At elevated pressures the oxidation rate of pure Si is dramatically increased since both the linear and parabolic rate constants in the Deal-Grove Si oxidation model are increased. The reason for the increase in the both of these constants can be seen directly from their definition which is given in the original work by Deal and Grove where the parabolic rate constant is defined as: $B=2D_{eff}C^*/N_1$ and the linear reaction rate constant is given by: $B/A=(khC^*)/((k+h))$ where N_1 is the number of oxidant molecules incorporated into a unit volume (i.e. a constant). It is the equilibrium concentration of oxidant in the oxide, C^*, which appears in both the linear and parabolic rate constants that is most greatly affected by increased pressure. At relatively low pressures the quantity C^* is linearly proportional to pressure and is given by Henry's law: $C^*=Kp$ where K is Henry's constant and p is the partial pressure of the oxidant. For non-ideal gases, p is replaced with fugacity which accounts for non-ideal gas behavior.

The high pressure technique allows technologically useful oxidation rates to be achieved at temperatures that are low enough to freeze the interdiffusion of Si and Ge even on a monolayer length scale. Thermodynamically, the application of up to 1000 atm (100 MPa) pressure has little effect on the free energy (and hence their activities) of condensed phases. This follows from the relative incompressibility, and the consequently small volume change, experienced by condensed phases under pressure. For ideal gases, on the other hand, the activity (fugacity) of each component is simply equal to its partial pressure and hence increases with increasing pressures. At low to moderate pressures ($0<P<100$ atm) the activity of gaseous oxygen is equal to its pressure in the reactor: $a_{O_2} = P_{O_2}$ where the standard state for a gas is defined by the pure gas at 1 atm. At much higher pressures ($P>500$ atm) the gas phase cannot be modelled as an ideal gas and the gas activity tends to increase even more rapidly with increasing pressure. The activity of a non-ideal gas at a particular pressure is given by its fugacity. Figure 1 shows the fugacity of oxygen as a function of gas pressure at a temperature of about 500°C. Note that as an added benefit of the high pressure approach, the activity (fugacity) of the reactant gas, increases non-linearly with pressure and, hence, the solubility of the oxidant (as given by Henry's Law) also increases. This directly affects the rate of the oxidation reaction at a given pressure.

Two oxidants, pure oxygen and water, were used separately and in combination in these experiments. The first apparatus was designed to use pure oxygen at pressures up to 2000 atm (200 MPa) and included a system for controllably adding moisture to the oxidizing environment. A second apparatus was designed and built to use water, above its critical temperature, as the principal oxidant species and is capable of achieving pressures greater than 1000 atm (100 MPa) independant of the oxidation temperature

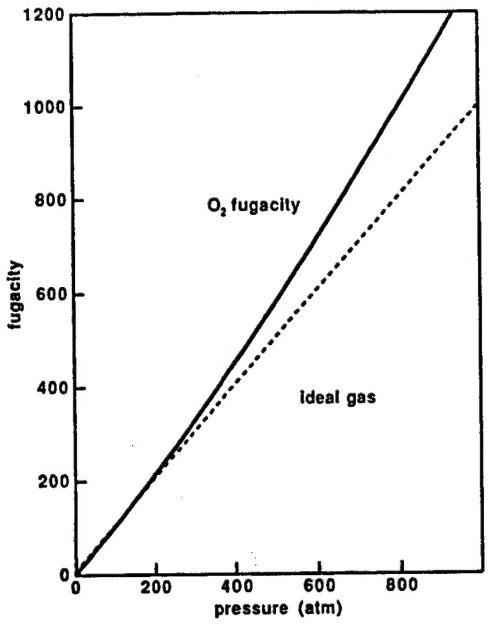

Figure 1: Plot showing the effect of increased pressure on the fugacity of oxygen.

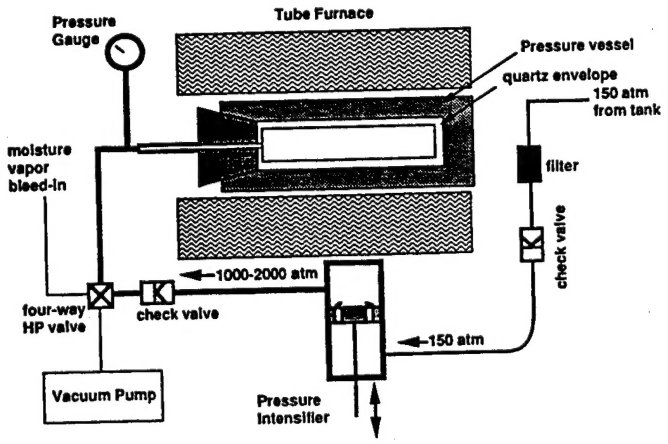

Figure 2: Schematic view of the high pressure dry oxygen system used in this work.

above the critical point. In both of these systems, because of the hot wall pressure vessel design, the maximum practical pressures are limited by the failure of the pressure vessel. Both systems are described below.

2.1.1 High Pressure Pure Oxygen System

A pure oxygen high pressure system was developed for the low temperature oxidation of $Si_{1-x}Ge_x$. The system is a closed, static gas pressure reactor that uses a quartz lined pressure vessel made from a high temperature alloy (Rene 41) which is rated for temperatures up to 650 °C at pressures up to 2,000 atm (200 MPa). The vessel is pressurized using a hand operated lubricant-free oxygen gas pressure intensifier. A schematic view of the system that we have constructed is shown in Fig. 2. Ultra high purity O_2 at near-tank pressure of 2500 psi is fed to an intensifier which is used to boost the pressure to the selected level. Multiple check valves in the process gas stream along with excess pressure burst disks are incorporated into the system for safety and to prevent backflow. The entire system, up to the tank regulator, is evacuated for a period of several hours to eliminate moisture from the system before pressurization. Fixed quantities of moisture can be introduced into the system (prior to pressurization) via a N_2 carrier gas that is bubbled through a temperature-controlled water bath. The reactor is heated via a tube furnace which is on linear bearings to enable rapid heating and cooling for additional process control.

2.1.2 Hydrothermal Oxidation

The hydrothermal method is a simple technique for achieving high oxidation potentials at low temperatures. We have explored the use of both open and closed systems. In the closed system, a fixed quantity of water is placed in a sealed pressure vessel which is heated above the critical transition where liquid and gas become indistinguishable. Through the use of common steam tables the appropriate water volume and vessel temperature to generate pressures of hundreds of MPa can selected. In Fig. 3, the fill factor (defined as the ratio of the volume of liquid water to the total vessel volume at 20°C) is plotted versus temperature for pressures between 20 and 60 MPa. Above the critical temperature, the fill factor is simply the density of the fluid state. Steam tables typically list the specific volume (m^3/kg) for a particular P-T condition which is easily converted into percent fill. On the right hand axis of Fig. 3, pressure (dashed line) is plotted for a 20% fill factor as a function of reactor temperature. Note that by filling the vessel to 20% of its volume with deionized water, the pressure in the reactor can be set by adjusting the temperature. Over the temperature range 350 to 650°C, the pressure in the vessel increases from 20 to 60 MPa. One can also set the desired reactor temperature and select a fill factor (left axis) to generate pressures over the same range. A wider range of pressures and temperature were achieved in this research through the use of direct pressurization of water at temperatures above the critical point. A system for doing this was designed and built that, in concept, is similar to the system shown in Fig. 2. The wet high pressure system consists of a unlubricated, compressed air-driven, hydrolic pump with teflon seals, a deionized water source, and a Rene 41 reactor vessel with a cold seal.

2.2 High pressure oxidation of $Si_{1-x}Ge_x$

A study of the kinetics of oxidation of $Si_{1-x}Ge_x$ in UHP oxygen at 70 MPa was undertaken. Oxide thickness was measured as a function of oxidation time and Ge alloy concentration. Figure 4 shows a plot of oxide thickness vs time for $Si_{0.85}Ge_{0.15}$ oxidized at 70 MPa in a static UHP oxygen atmosphere. As expected, the oxidation rate at 550°C is faster than at 500°C. We also investigated the effect of oxidation in flowing oxygen at similar pressures. These studies revealed a significant increase in the oxidation rate over static conditions. We attribute this to the increased presence of moisture in the reactor vessel which, even at a level of ≈20 ppm, appears to have a dramatic effect on the kinetics of thermal Si oxidation in both the linear and parabolic regimes. We have also observed a strong effect of Ge concentration on the rate of oxidation at 70 MPa. This is shown in Fig. 5 which presents thickness vs time data for 10 and 15 at.% Ge samples oxidized at 550°C. For each pair of data points, samples were placed side-by-side in the oxidation reactor, and hence were exposed to identical conditions. In addition, for some of the runs, pure Si samples were placed in the reactor. In the case of pure Si, no measurable oxide growth was observed under the conditions used to produce the data in Fig. 5. Note that the rate of oxidation in the 15 at.% Ge case was greater than the rate for 10 at.%. This suggests that Ge plays a significant role in the oxidation process probably by increasing the diffusivity of the oxidant in the oxide.

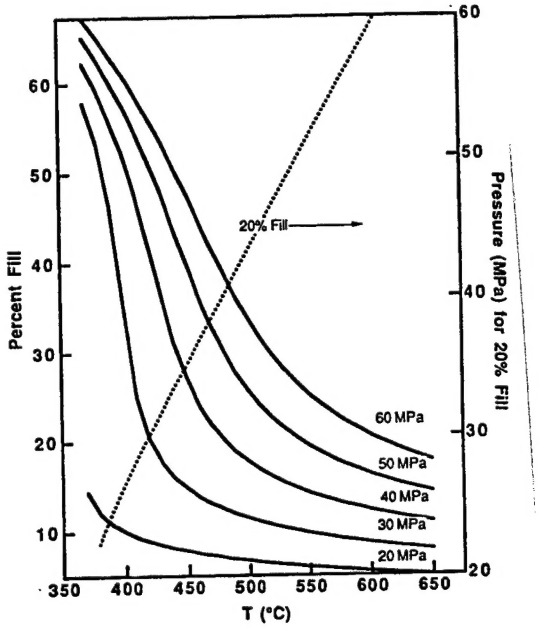

Fig. 3: Conventional steam table isobars between 20 and 60 MPa plotted in terms of fill factor. On right hand axis the pressure in a 20% by volume filled vessel is shown.

Detailed compositional analysis from XPS data (from both Ar ion sputter cleaned and uncleaned samples) show that the relative Si-Ge composition of the oxide is identical to that of the underlying alloy for both the 10 and 15 at.% samples. Of equal importance is the chemical state of the Ge in the oxide which was analyzed using a Gaussian curve fitting routine to analyze the Ge_{2p3}-peak in the XPS spectra. An unoxidized $Si_{1-x}Ge_x$-alloy sample was used to provide a calibration for the position of the elemental Ge XPS peak. An XPS spectrum obtained from a 50 nm thick HPO oxide (dry O_2, 500°C, and 70 MPa) grown on a 150 nm thick $Si_{0.85}Ge_{0.15}$ alloy film shows that the Ge_{2p3} peak is consistent with a bonding configuration for GeO_2 (1220.40 eV) and, to a lesser extent, GeO. Importantly,

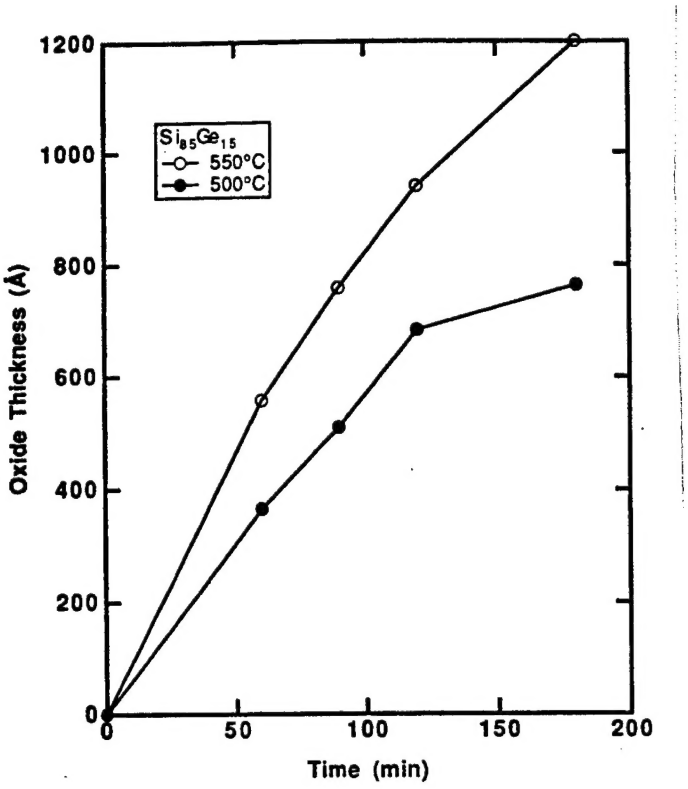

Figure 4: Plot of oxide thickness versus time for $Si_{0.85}Ge_{0.15}$ oxidized at 70 MPa in a static dry oxygen atmosphere.

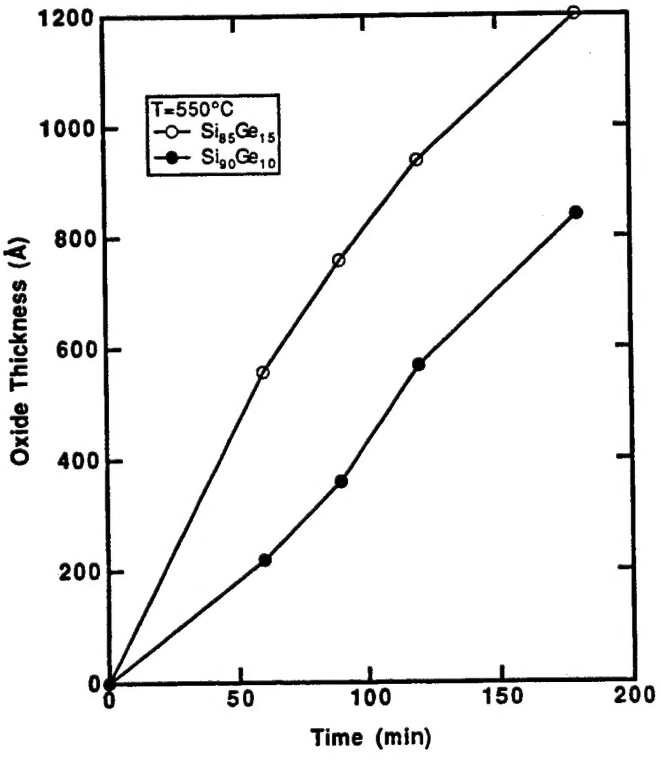

Figure 5: Plot of thickness versus time for 10 and 15 at% Ge samples oxidized at 550°C.

there is no detectable elemental Ge peak (1217.20 eV) in the XPS spectra which shows that Ge was chemically incorporated into the oxide. Similar results were obtained from oxides grown from alloys in the compositional range 10 to 40 at%.

The importance of interface morphology has been demonstrated in the Si/SiO_2 system where the presence of interfacial hillocks or asperities in thin gate oxides used in MOS devices results in premature dielectric breakdown, a reduction in channel carrier mobility, and an increase in interface states. We have used high resolution TEM to evaluate the interface planarity of the $Si_{1-x}Ge_xO_2/Si_{1-x}Ge_x$ interface formed by HPO. A high resolution TEM image of an HPO oxide/$Si_{0.85}Ge_{0.15}$ alloy interface oriented so that the substrate <110> direction is parallel to the incident electron beam is shown in Fig. 6. This figure shows that there is an abrupt transition from amorphous to crystalline contrast at the oxide/alloy interface. Variations in the planarity of the interface appear to be no greater than 1-2 monolayers in amplitude and the interface morphology is qualitatively comparable to that which is reported for Si/SiO_2 interfaces used in MOS devices. This result combined with detailed Raman spectroscopy studies show that Ge does not accumulate at the interface using this process.

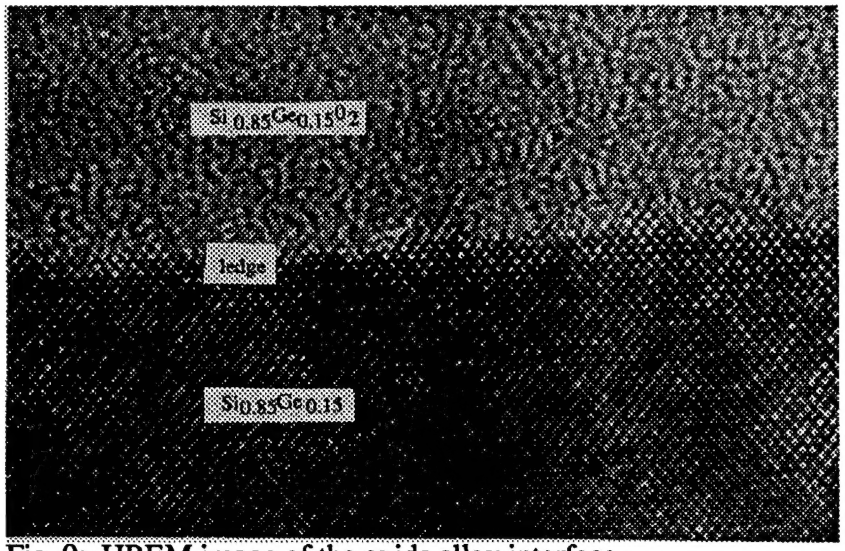

Fig. 9: HREM image of the oxide alloy interface.

High frequency 1 MHz C-V curves were measured from Al metallized structures fabricated from alloys of 10 and 15 at.% Ge oxidized using the HPO conditions previously described. There was no observable hysteresis displayed for curves obtained from 10 and 15 at% sample. Samples containing higher Ge concentration (up to 40 at%) were not of high enough electronic quality to allow meaningful measurements to be obtained. The high frequency C-V plots were, as compared to the ideal curve, elongated along the voltage axis corresponding to a continuous distribution of states in the band gap. The high frequency or Terman method was used to estimate the number of states associated with the observed elongation.

Based on the Terman method, the midgap interface state density was estimated to be about 1×10^{12} cm^{-2} eV^{-1} for both the 10 and 15 at.% samples. The total charge per unit area induced in the semiconductor by charges in the dielectric layer, (Q_s), was estimated by a charge analysis method which is described in detail elsewhere. Using this approach, the flatband voltage (V_{FB}) shift of the experimentally measured C-V curve was determined and the induced charge, Q_s, was estimated using:

$$Q_s = (-V_{FB} + \phi_{ms}) * C_0$$

where ϕ_{ms} is the appropriate metal-semiconductor work function difference, and C_0 is the capacitance per unit area of the dielectric layer. It should be emphasized that this value of Q_s cannot be unambiguously associated with Q_f (oxide fixed charge). This would only be the case in the absence of interface states. In fact, it is very difficult to distinguish the Q_f charge component and the interface state density component from one another. Such a separation requires detailed information about the nature and distribution of D_{it}.

Analysis of C-V curves from 10 and 15 at% Ge alloys reveals a V_{FB} shift which can be attributed to Q_s /q, in the 10 at.% Ge case, of positive +1 x $10^{11}cm^{-2}$ (negative V_{FB}) and, in the 15 at.% case, of negative -1 x $10^{12}cm^{-2}$ (positive V_{FB}). The origin of these large differences is difficult to unambiguously determine from the present data. However, previous studies of conventionally oxidized, dilute $Si_{1-x}Ge_x$ alloys have shown large positive V_{FB} shifts in C-V curves similar to that seen in the 15 at.% sample. In the previous work, these shifts were largely attributed to the existence of a large negative Q_f resulting from intermediate Si oxidation states and elemental Ge at the Si/SiO_2 interface. It is also known that GeO_2 rather readily becomes oxygen deficient which can result in the formation of deep level electron traps. Such electron traps would result in a high level of Q_{ot} (oxide trapped charge) and, if these charges are in electrical communication with the underlying semiconductor, an increase in D_{it} as well. Forming gas anneals result in a decrease in both Q_s and D_{it} in all of the measured oxides.

After optimization of the oxidation temperature, pressure, and post-oxidation annealing (H_2/N_2) we were able to reduce the interface states density (D_{it}) of the aluminium metallized samples to the $1x10^{12}/eVcm^2$ range. Due to unacceptably high leakage current through the oxide we were unable to use the more accurate quasi-static method to obtain D_{it} in these structures. The origin of the leakage current appears to be associated with a high density of Ge E' centers in the oxide. The presence of these centers in a concentration of about $1x10^{18}$ $/cm^3$ in our HPO $Si_{1-x}Ge_x$ oxides was established through a collaboration with Prof. Mary Ellen Zvanut at U. of A. To eliminate the problem of the high I_L several different layered structures were fabricated using plasma CVD to deposit layers of Si_3N_4 and SiO_2 at low temperatures (250-300°C) on top of the high pressure oxides. The typical conditions for the fabrication of these layered devices is to first grow 35 nm of high pressure oxide on top of which we plasma deposit layers of similar thickness of nitride and oxide to form: $Al \mid SiO_2 \mid Si_3N_4 \mid Si_{0.9}Ge_{0.1}O_2 \mid Si_{0.9}Ge_{0.1}$ capacitors. In these ONO-type structures D_{it} values of $5\text{-}10x10^{11}/cm^2eV$ and a leakage current of $5x10^{-9}$ A/cm^2 were typical.

The basic concept of thermal oxidation of SiGe for the purpose of forming an oxide that is compositionallly congruent with the underlying material hasd been proven. The electronic properties of the as grown oxide in terms of interface states densities, dielectric breakdown strength, and leakage have been dissapointing. The source of these problems appears to be two fold. The first problem is fundamental; there is evidence that the incorporation of Ge in the oxide results in enhanced leakage due to carrier hopping from E' centers. This problem requires further study but, as shown in our work, can be alleviated by deposing a caping nitride/oxide layer onto the thermally grown SiGe. The second problem is technological and is the result of the design of the high pressure system. The system consists of an externally heated pressure vessel that has a quartz envelope that contains the sample. During heating at high pressure the vessel, consisting of Rene 41 alloy is partially oxidized by the ambient and metal ions diffuse along surfaces and through

the quartz envelope to contaminate the specimen with metal ions detected using Auger Electron Spectroscopy . These ions clearly contribute to the relatively poor electronic performance of the oxide.

2.3 Synthesis of Nanocrystalline Ge from High Pressure $Si_{1-x}Ge_x$-oxides

High pressure techniques can be used for low temperature oxidation of alloys of $Si_{1-x}Ge_x$ to form compositionally congruent oxides of $Si_{1-x}Ge_xO_2$. The oxides formed in this manner have been shown in this work to be a uniform solid solution of SiO_2 and GeO_2. The latter species can be chemically reduced to elemental Ge via reaction with, for example, H_2 or Si to produce a uniform distribution of Ge precipitates embedded in an SiO_2 matrix. This novel synthesis route is of interest for use in studies of the fundamental physical properties of nanocrystalline indirect semiconductors. For instance, visible photoluminescence from indirect band-gap materials has been reported from porous Si [1] from nanocrystalline Ge [2] and from lithographically patterned planar Ge structures [3]. We have shown that H_2 can be used to chemically reduce GeO_2 in $Si_{1-x}Ge_xO_2$ oxide alloys to form elemental Ge precipitates embedded in an SiO_2 matrix. This process, however, also removes oxygen from the oxide network in the form of H_2O which must diffuse from the reaction site to the atmosphere. The reduction reaction can be written as follows:

$$GeO_{2(\text{in solid solution with } SiO2)} + H_{2(v)} = Ge + H_2O_{(v)}$$

Using Gibbs free energy of formation data for hexagonal GeO_2, the standard Gibbs Free energy of reaction for the H_2 reduction is estimated to be between -5 and -11 kJ/mole in the temperature range between 750 and 850 °C. From this it is straightforward to calculate that the equilibrium ratio of P_{H2O}/P_{H2} (which sets the oxidation potential) above which this reaction will not proceed is between 0.9 and 7 over this temperature range. This is illustrated in Fig. 7 which shows a plot of equilibrium P_{H2O}/P_{H2} as a function of temperature. There are three distinct phase fields in this figure, one in which neither SiO_2 nor GeO_2 are reduced, one in which only GeO_2 reduced, and one in which both SiO_2 and GeO_2 are reduced. Note that there is a wide range of oxygen activities (P_{H2O}/P_{H2}) over which only GeO_2 is reduced. In fact, it is well known that the reduction of SiO_2 with H_2 at 1 atm is not a practical process below 1100 °K. On the other hand, the upper boundary of the GeO_2 reduced phase field is well

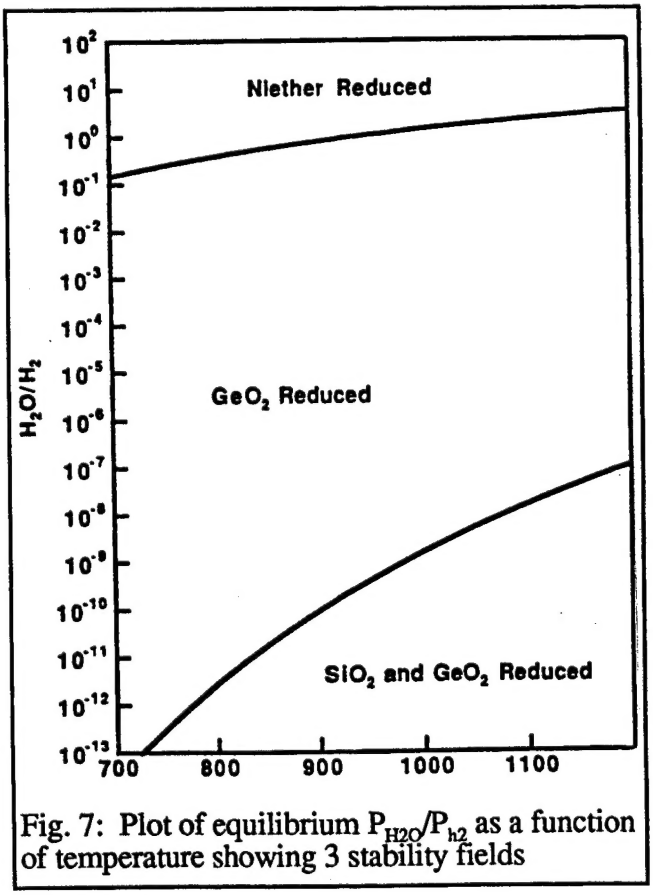

Fig. 7: Plot of equilibrium P_{H2O}/P_{h2} as a function of temperature showing 3 stability fields

within the oxygen activity level that can be readily obtained experimentally.

In the as-grown condition the oxides formed using the hydrothermal method described above consist of an approximately 800 nm thick region of $Si_{60}Ge_{40}O_2$ with a 250 nm thick underlying SiO_2 layer. Cross-sectional TEM images initially show uniform amorphous contrast across the oxide thickness with no evidence of SiO_2-GeO_2 phase separation. After extended exposure to the 120 keV electron beam the oxide takes on a mottled amorphous contrast that suggests electron-beam-induced phase separation. For this reason extended exposure to the 120 KeV beam was avoided in these TEM studies.

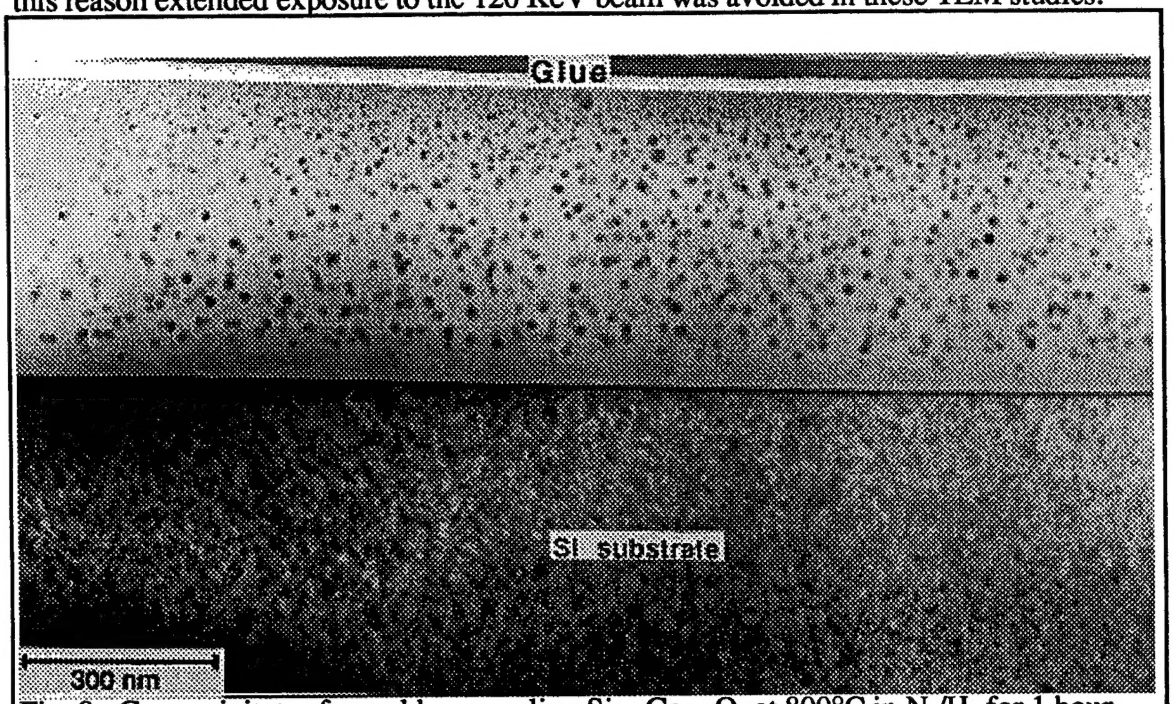

Fig. 8: Ge precipitates formed by annealing $Si_{0.60}Ge_{0.40}O_2$ at 800°C in N_2/H_2 for 1 hour.

The effect of annealing a $Si_{60}Ge_{40}O_2$ sample at 800 °C for 1 hour in forming gas is shown in the cross-sectional TEM image presented in Fig. 8. In this figure there are Ge precipitates visible through the entire original $Si_{60}Ge_{40}O_2$ layer. These precipitates range in size from about 1 to 120 nm in diameter. Studies of the precipitate distribution at increasing time at temperature show that the precipitation reaction proceeds via the translation of a precipitation front which starts at the surface and moves through the thickness of the oxide at a rate which is controlled by a thermally activated process. A high resolution TEM image taken from the 800°C, 60 min sample is presented in Fig. 9 and shows a typical particle.

The activity of water in the oxide will depend on the rate at which it can diffuse out of the oxide. Since diffusion of H_2O species [4] is significantly slower than the diffusion of H_2 species [5] in silicon oxide this suggests that the reaction is rate limited by out-diffusion of H_2O species. In this discussion, the nature of the diffusing water species is not considered. The position of the interface between the precipitated region and the precipitate-free region in samples annealed in forming gas was used to estimate that the H_2O diffusion rates are at least three orders of magnitude faster than is predicted by published diffusion data. In this calculation, the activity of H_2O at the precipitation front is assumed to be set by the reaction equilibria and the concentration of H_2O at the oxide

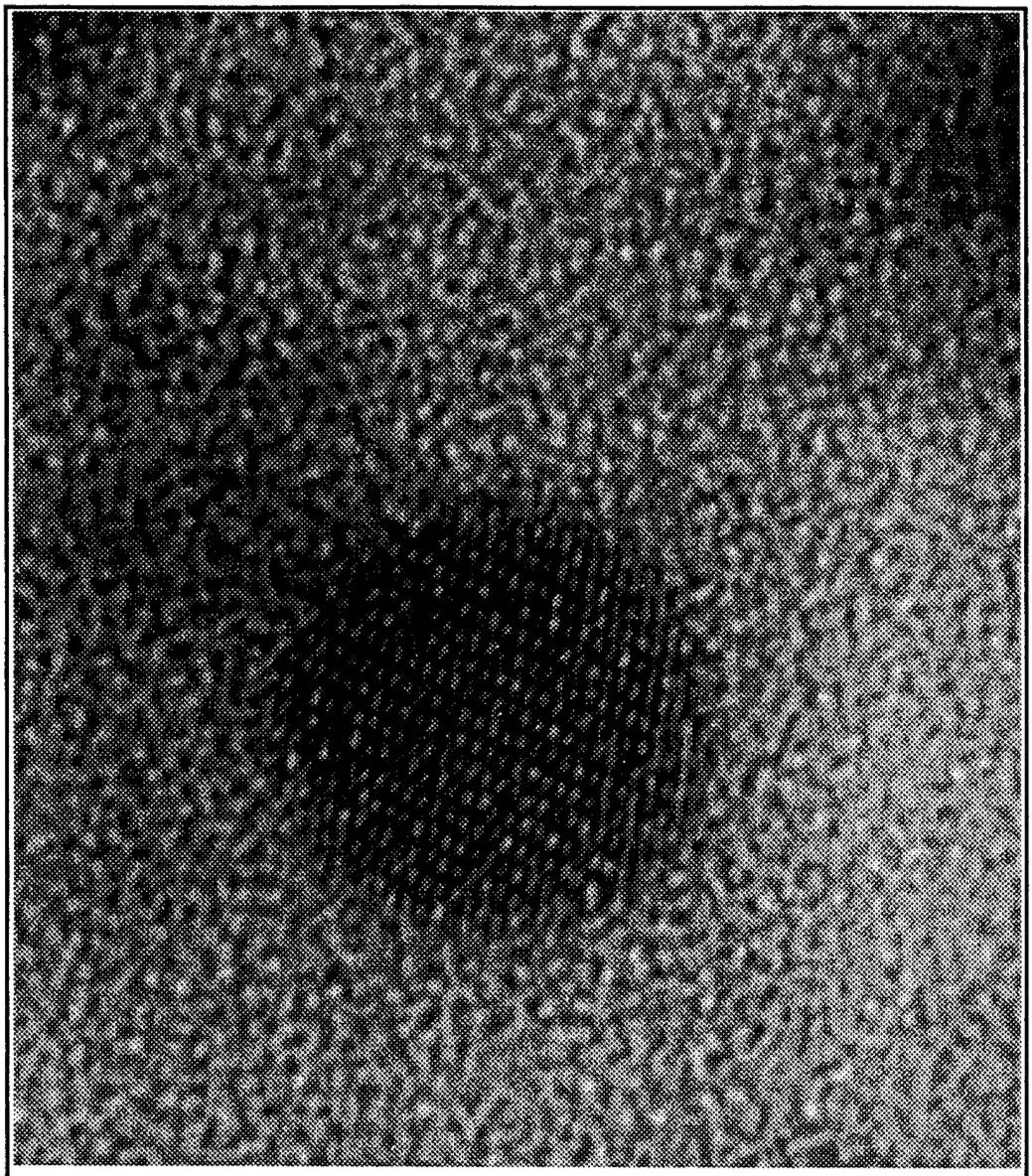

Fig. 9: HREM image of a Ge nanocrystal formed by chemical reduction.

surface is assumed to be zero. The presence of water species both in the gas phase and in the oxide has a significant effect on the driving force for the precipitation reaction and thus it is instructive to calculate the dependence of the critical particle radius on P_{H_2O}/P_{H_2} using classical nucleation theory [7]. In this case, the free energy that provides the driving force for the Ge precipitation reaction is given by $\Delta G=\Delta G^{\circ} + RT\ln(a_{H_2O}/a_{H_2})$, where a_{H_2O}/a_{H_2} is the ratio of the activities of H_2O and H_2 dissolved in the amorphous solid. For this qualitative analysis, we replace the dissolved activity ratio with the gas phase activity ratio P_{H_2O}/P_{H_2} and will assume that the surface energy of the Ge particles in SiO_2 is less than or equal to the surface energy (γ) of Ge near its melting point (γ=0.6 J/m^2). With these assumptions we have used the expression $r^*=2\gamma/\Delta G$ to calculate the critical particle radius (r^*) as a function of P_{H_2O}/P_{H_2} and temperature which is shown in Fig. 10. The trend is clear from this figure, as the equilibrium water vapor pressure is approached, the driving

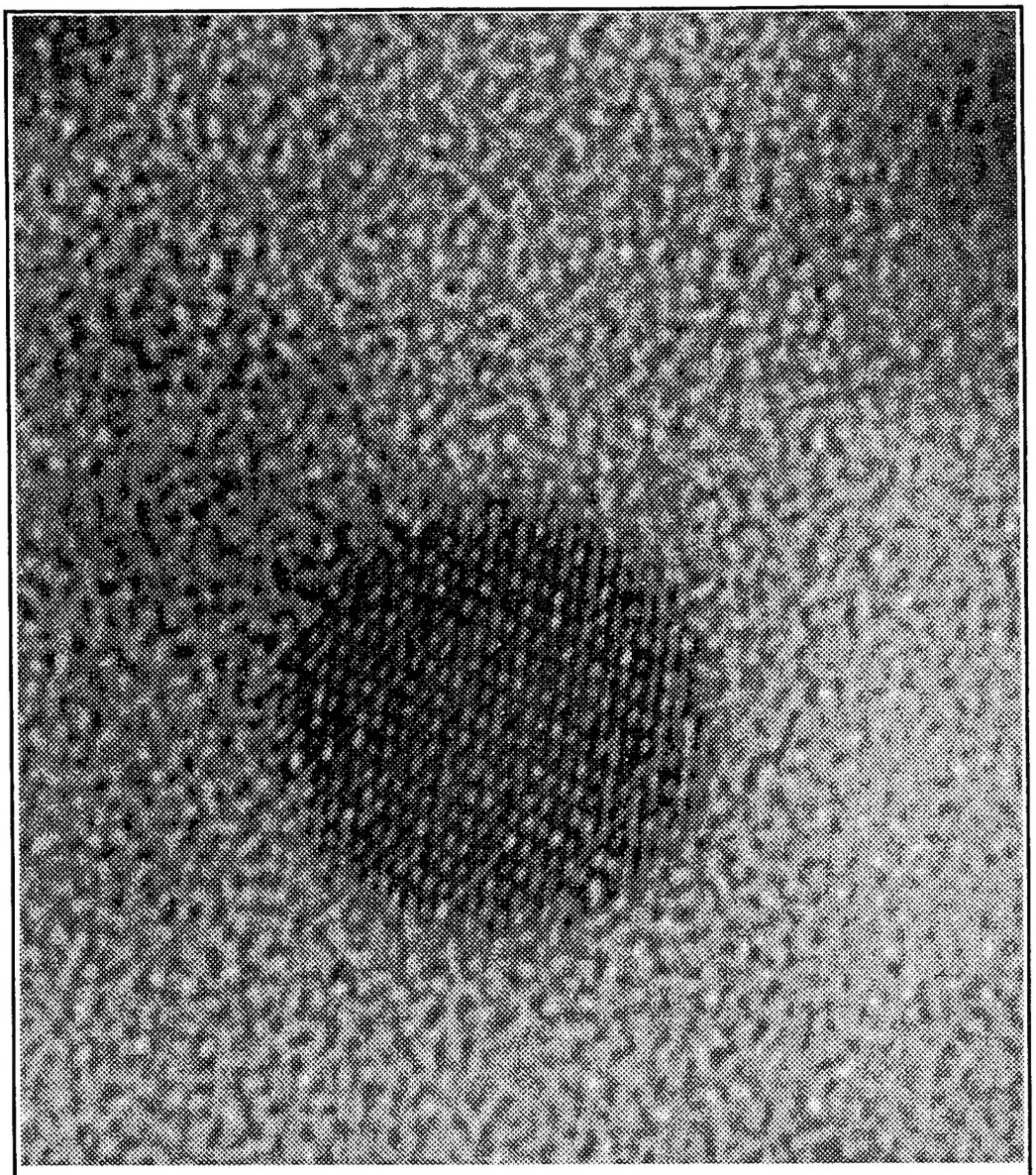

Fig. 9: HREM image of a Ge nanocrystal formed by chemical reduction.

surface is assumed to be zero. The presence of water species both in the gas phase and in the oxide has a significant effect on the driving force for the precipitation reaction and thus it is instructive to calculate the dependence of the critical particle radius on P_{H_2O}/P_{H_2} using classical nucleation theory [7]. In this case, the free energy that provides the driving force for the Ge precipitation reaction is given by $\Delta G=\Delta G^{\circ} + RT\ln(a_{H_2O}/a_{H_2})$, where a_{H_2O}/a_{H_2} is the ratio of the activities of H_2O and H_2 dissolved in the amorphous solid. For this qualitative analysis, we replace the dissolved activity ratio with the gas phase activity ratio P_{H_2O}/P_{H_2} and will assume that the surface energy of the Ge particles in SiO_2 is less than or equal to the surface energy (γ) of Ge near its melting point (γ=0.6 J/m^2). With these assumptions we have used the expression $r^*=2\gamma/\Delta G$ to calculate the critical particle radius (r^*) as a function of P_{H_2O}/P_{H_2} and temperature which is shown in Fig. 10. The trend is clear from this figure, as the equilibrium water vapor pressure is approached, the driving